FigS1

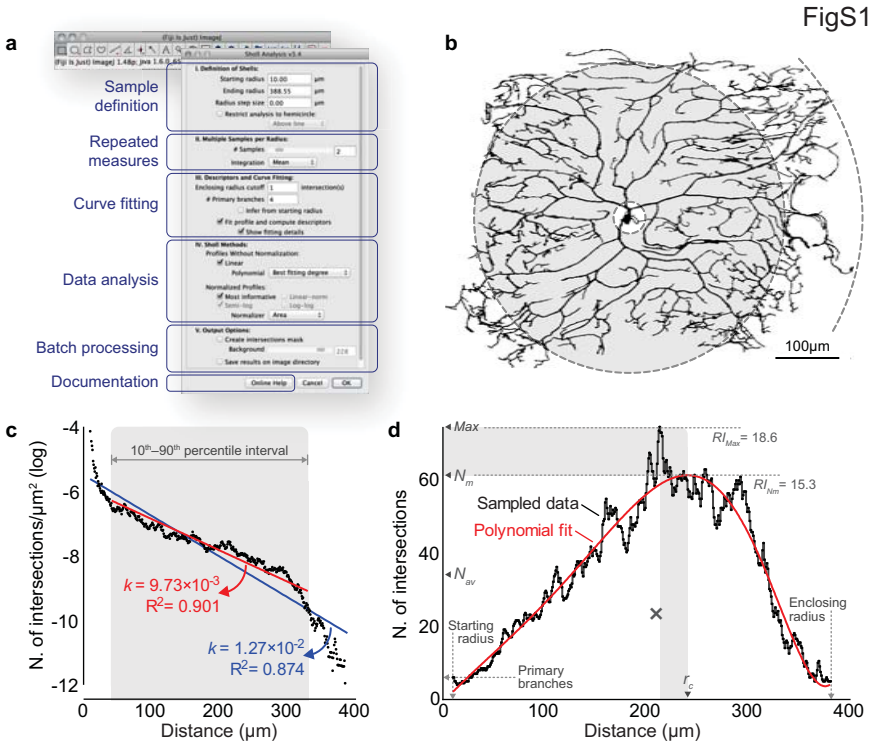
a
Sample definition
Repeated measures
Curve fitting
Data analysis
Batch processing
Documentation
b
100µm
c
10th–90th percentile interval
k = 9.73×10-3
R2= 0.901
k = 1.27×10-2
R2= 0.874
N. of intersections/µm2 (log)
Distance (µm)
d
Max
Nm
Nav
RIMax= 18.6
RINm= 15.3
Sampled data
Polynomial fit
Starting radius
Primary branches
Enclosing radius
rc
N. of intersections
Distance (µm)

FigS2

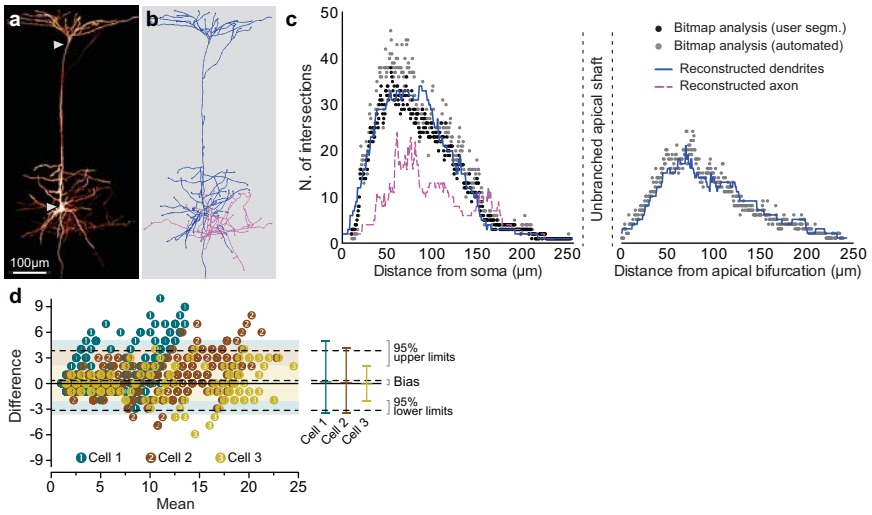
a
b
c
d
100µm
N. of intersections
Distance from soma (µm)
Unbranched apical shaft
Distance from apical bifurcation (µm)
Bitmap analysis (user segm.)
Bitmap analysis (automated)
Reconstructed dendrites
Reconstructed axon
Difference
Mean
Cell 1
Cell 2
Cell 3
95% upper limits
Bias
95% lower limits

FigS3

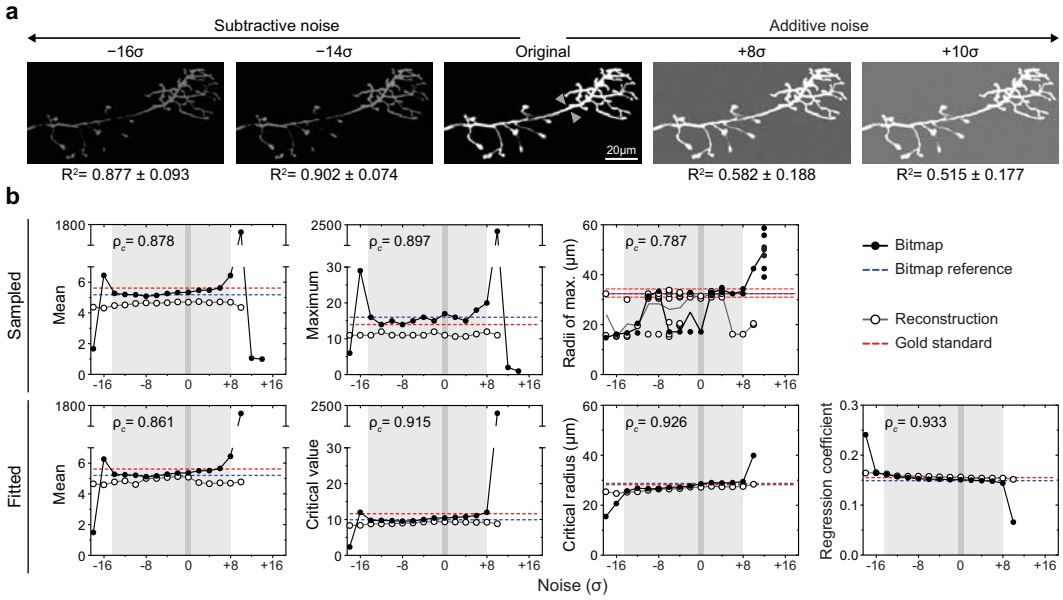
a
Subtractive noise
Additive noise
−16σ
−14σ
Original
+8σ
+10σ
20μm
R²= 0.877 ± 0.093
R²= 0.902 ± 0.074
R²= 0.582 ± 0.188
R²= 0.515 ± 0.177
b
Sampled
Fitted
Mean
Maximum
Radii of max. (μm)
Critical value
Critical radius (μm)
Regression coefficient
ρc= 0.878
ρc= 0.897
ρc= 0.787
ρc= 0.861
ρc= 0.915
ρc= 0.926
ρc= 0.933
Bitmap
Bitmap reference
Reconstruction
Gold standard
Noise (σ)

FigS4

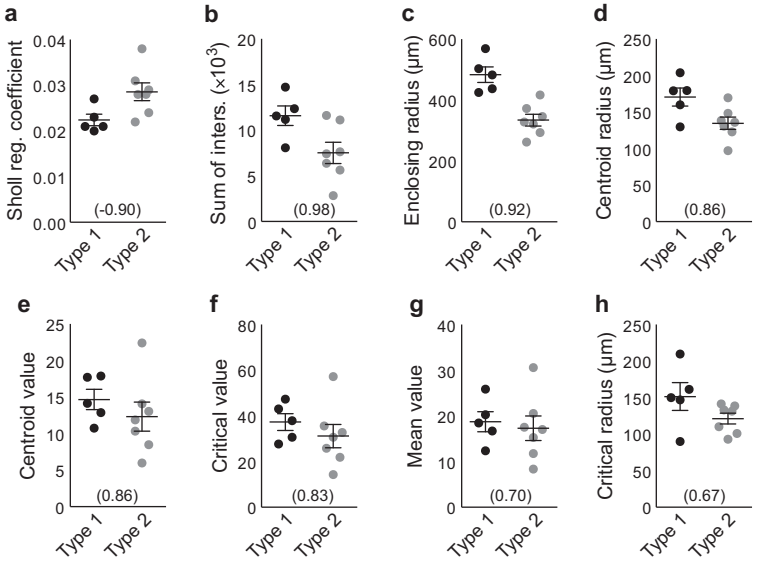
a
Sholl reg. coefficient
0.04
0.03
0.02
0.01
0.00
(-0.90)
Type 1
Type 2
b
Sum of inters. (×10^3)
20
15
10
5
0
(0.98)
Type 1
Type 2
c
Enclosing radius (µm)
600
400
200
0
(0.92)
Type 1
Type 2
d
Centroid radius (µm)
250
200
150
100
50
0
(0.86)
Type 1
Type 2
e
Centroid value
25
20
15
10
5
0
(0.86)
Type 1
Type 2
f
Critical value
80
60
40
20
0
(0.83)
Type 1
Type 2
g
Mean value
40
30
20
10
0
(0.70)
Type 1
Type 2
h
Critical radius (µm)
250
200
150
100
50
0
(0.67)
Type 1
Type 2

Supplementary Information

Neuronal morphometry directly from bitmap images

Tiago A. Ferreira, Arne V. Blackman, Julia Oyrer, Andrew J. Chung, Sriram Jayabal, Alanna J. Watt, P. Jesper Sjöström, Donald J. van Meyel

Contents

Supplementary Figures

Supplementary Figure 1. Overview of the *Sholl Analysis* software.

(a) User interface, version 3.4. Sub-modules noted in blue.

(b) Maximium intensity projection of a Drosophila class IV dendritic arborization sensory neuron (ddaC) labeled by the *ppk1.9-GAL4*-driven reporter *UAS-mCD8::GFP*, a sample image distributed with the plug-in. The annulus formed by *Starting radius* (the first sampled distance) and *Critical radius* is indicated. Outer arc depicts *Enclosing radius*, the distance to the most distal dendritic tip.

(c) Semi-log plot of the cell depicted in (b), where the number of intersections was normalized to the area of each sampled shell. Two regression lines are shown to demonstrate that curves can be fitted to all data points, or to a subset restricted to the 10^{th} to 90^{th} percentiles of the data (shaded in gray). R^2 is the coefficient of determination, and *k* the *Sholl regression coefficient*.

(d) Linear Sholl plot of the cell in (b). Key metrics include *Critical value* (N_m), *Critical radius* (r_c) and *Mean value* (N_{av}). Differences between sampled and fitted maxima are shaded in gray. The centroid of the sampled profile is marked (×). *Schoenen ramification index* (*RI*) is the ratio between number of branches at the maximum and the number primary branches, using either sampled data or the fitted N_m. The number of primary branches can be entered manually, or drawn from the number of intersections at *Starting radius.*

Supplementary Figure 2. Accuracy of bitmap image-based *Sholl Analysis*.

(a) Maximum intensity projection of an Alexa 594 dye-filled layer-5 pyramidal neuron of juvenile mouse visual cortex[1]. Arrowheads highlight the apical tuft (top) and the soma (bottom).

(b) Manually reconstructed dendrites (blue) and axon (magenta) of the neuron in (a).

(c) Linear Sholl plots from bitmap images (dots), following either manual segmentation ("user segm.") or automated segmentation of the image stack. For comparison, results from reconstruction-based analysis are plotted for the axon (dashed magenta line) and dendrites (solid blue line). The plot of the left corresponds to the basal region populated by both axonal and dendritic arbors, while the plot on the right corresponds to apical dendrites.

(d) Bland-Altman plot to examine the agreement between the bitmap approach and traced reconstruction approach for three different neurons (numbered and color-coded). Each data point represents the count of intersections at a particular distance from the apical

bifurcation: pairwise differences between the two approaches at each distance are plotted against each mean. The 95% limits of agreement for individual cells are shown to the right, as is the average for all three cells and the average bias (dotted lines).

Supplementary Figure 3. Resilience of bitmap image-based morphometry to image degradation over a range of synthetic noise.

(a) Maximum intensity projection of an axonal arbor of a Drosophila olfactory projection neuron from the DIADEM Challenge dataset (*OP_1*)[2, 3]. We contaminated the original stack (voxel size: 0.33×0.33×1.0μm) with Poisson noise, using increasing multiples of the stack standard deviation ($\sigma = 9.55$) as the probability mass function of the Poisson random variable. This noise was either added (+) or subtracted (−), over a range from -18σ to $+18\sigma$. Images are shown with the coefficient of determination below each image (R^2, mean ± s.d.) to indicate the degree of similarity with the original; $R^2 = 1$ corresponds to identical images. Arrowheads indicate the Sholl analysis center (see b).

(b) Each graph represents one of 7 metrics (3 from sampled data, 4 from fitted data) that were calculated from Sholl plots generated directly from bitmap images with *Sholl Analysis* ("Bitmap"), or from their respective reconstructions traced with *Neural Circuit Tracer*[4] ("Reconstruction"). The parameters and routines used to retrieve the data were fixed (See **Supplementary Methods** and **Supplementary Files** for details). Shaded areas in each graph (light gray) indicate the range of noise (-14σ to $+8\sigma$) over which metrics were largely consistent with those calculated from the original image (zero noise, dark grey vertical bar). Dashed lines indicate two references calculated at zero noise: one from a user-derived manual segmentation of the stack ("Bitmap reference", blue) and one from the DIADEM gold standard reconstruction (red). For each metric, the concordance correlation coefficient (ρ_c)[5] between the bitmap approach and reconstruction approach are shown.

Supplementary Figure 4. Sholl-based metrics of Type-1 and Type-2 PV interneurons.

Metrics loading on the first principal component (71.6% of observed variation), used as clustering variable in **Fig. 1c**: **(a)** Sholl regression coefficient, **(b)** Sum of intersections, **(c)** Distance associated with at least two intersections (a modified *Enclosing radius*), **(d)** Centroid radius, **(e)** Centroid value, **(f)** Critical value, **(g)** Mean value, **(h)** Critical radius. Values enclosed by brackets depict factor loadings. Because pipette fluorescence could not be entirely eliminated near the soma, the *number of primary branches* and *Schoenen ramification indices* were excluded from the analysis.

Supplementary Methods

Programming

Programming was performed with Eclipse SDK 3.7.2 (Eclipse Foundation) and Fiji's built-in Script Editor. The source code of *Sholl Analysis* is available through the plug-in's internet documentation page (http://fiji.sc/Sholl_Analysis).

Image Acquisition

Images acquisition has been described previously for Drosophila sensory neurons[6], and for neocortical pyramidal cells and PV interneurons[1]. Neocortical cells were visualized in P12–P20 acute mouse visual cortex slices using custom-built 2-photon imaging workstations (Scientifica UK) with ScanImage[7] v3.7 running in MATLAB (MathWorks). Two-photon excitation of Alexa-594 loaded via the patch pipette was obtained with a Ti:Sa laser (Spectraphysics MaiTai or Coherent Chameleon) tuned to 800–820nm, and data was acquired with Hamamatsu R3896 bi-alkali detectors and National Instruments PCI-6110 digitization boards. All recordings were in neocortical layer 5, as determined by the presence of conspicuous large pyramidal somata with characteristic apical dendrites, as visualized by Dodt contrast. PV interneurons were targeted in slices from GFP-expressing G42 mice[8] by tuning laser to 880–900nm and visualizing GFP fluorescence.

To produce Purkinje cell-specific expression of Brainbow, transgenic Pcp2-cre mice (Jackson Laboratory) were crossed to Brainbow 2.1 mice (line R, Jackson Laboratory). Five-month-old progeny were deeply anaesthetized (Ketamine/Xylazine, 80/5 mg/kg), and perfused with 4% paraformaldehyde. Sagittal brain slices were cut 24 hours later from the cerebellar vermis (100 µm thick) using a Leica Vibratome 1000S, and mounted with Prolong Gold Antifade (Invitrogen). Images were collected with an Olympus confocal microscope with a 60X oil immersion objective (NA= 1.35), using the following laser wavelengths: 559nm, 515nm, and 440nm. Images (512 X 512 pixels) were acquired using a z-axis step of 0.5µm and were deconvolved with AutoQuant software (Media Cybernetics).

Image Processing

Image processing was performed in Fiji[9]. Image fields were stitched together[10], and fluorescence signal from filling pipettes and dye spillage (PV cells) or fluorescence artifacts (Brainbow cells) was eliminated manually. Background was eliminated through 3D median filtering (typically radius=2–3), and stacks were segmented using one of ImageJ's built-in threshold methods. Due to diminished brightness, some image stacks were enhanced with the *Tubeness* plug-in (http://fiji.sc/Tubeness)[11]. Subsequently, bitmap Sholl was performed as described in the Batch Processing section of the *Sholl Analysis* internet documentation page, which contains most of the image processing routines used in this study.

Reconstructions were performed using Neuromantic[12] or, in the case of Brainbow tissue, with Neurolucida (MicroBrightField, Inc.). Neurolucida tracings were converted to the SWC format[13] using L-Measure[14]. Reconstructions were imported into Simple Neurite Tracer[11] using the appropriate coordinate offset so that the tracings would align optimally with the corresponding bitmap image. The Sholl technique for these reconstructions was performed using Simple Neurite Tracer, using a manually chosen point as the center of analysis. The closest voxel to this point was chosen for subsequent bitmap *Sholl Analysis*. For consistency, data was obtained using the minimum sampling distance allowed by the bitmap approach, i.e., the cube root of the product of the voxel dimensions.

Automated reconstructions of DIADEM projections were performed in Neural Circuit Tracer 2.0[4]. Scripts and instructions on how to process the DIADEM *OP_1* dataset are available as **Supplementary Files**.

Data Analysis

For Bland-Altman plots[15] of pyramidal cell apical dendrites, profiles were obtained as described above, using the main apical bifurcation as the center of analysis. Pairwise comparisons were performed at each sampled distance. Bias was calculated as the average of the differences between the two methods. Limits of agreement were calculated as bias ±1.96 times the standard deviation of the differences.

For each neuron, we retrieved all the metrics calculated by the *Sholl Analysis* plug-in and performed clustering analysis following Principal Component Analysis as described elsewhere[16, 17] (**Supplementary Fig. 4**). The first component (which accounted for 71.6% of the observed variation) was used as clustering variable. Hierarchical clustering was performed using Ward's method and squared Euclidean distances as linkage metric. A 25% linkage cutoff, as normalized to the greatest separation in the data set, was used as a best-cut selection criterion for the number of found clusters[17]. Analyses were performed in JMP 10.0 (SAS Institute) and Prism 5.0 (Graphpad Software).

Supplementary Files

Processing routines for the OP_1 DIADEM dataset (related to Supplementary Figure 3).

Scripts used to obtain the data presented on Supplementary Fig. 3: ImageJ macros (OP_1_NoiseTest.ijm and OP_1_UserSeg.ijm) and Neural Circuit Tracer macro (OP_1_NCTracer.macro) used for automated reconstruction of the OP_1 image**.**

Supplementary References

1. Buchanan, K.A. et al. *Neuron* **75**, 451-66 (2012).
2. Brown, K.M. et al. *Neuroinformatics* **9**, 143-57 (2011).
3. Jefferis, G.S. et al. *Cell* **128**, 1187-203 (2007).
4. Chothani, P. et al. *Neuroinformatics* **9**, 263-78 (2011).
5. Lin, L.I. *Biometrics* **45**, 255-68 (1989).
6. Ferreira, T.A. et al. *Development* (2014, in press: doi:10.1242/dev.099655).
7. Pologruto, T.A. et al. *Biomed Eng Online* **2**, 13 (2003).
8. Chattopadhyaya, B. et al. *J Neurosci* **24**, 9598-611 (2004).
9. Schindelin, J. et al. *Nat Methods* **9**, 676-82 (2012).
10. Preibisch, S. et al. *Bioinformatics* **25**, 1463-5 (2009).
11. Longair, M.H. et al. *Bioinformatics* **27**, 2453-4 (2011).
12. Myatt, D.R. et al. *Front. Neuroinform.* **6**, 4 (2012).
13. Ascoli, G.A. et al. *Anat. Embryol.* **204**, 283-301 (2001).
14. Scorcioni, R. et al. *Nat Protoc* **3**, 866-76 (2008).
15. Bland, J.M. & Altman, D.G. *Lancet* **1**, 307-10 (1986).
16. Kozloski, J. et al. *Science* **293**, 868-72 (2001).
17. Everitt, B. Cluster analysis, Edn. 5th. (Wiley; 2011).